

Journal of Materials Chemistry A

Accepted Manuscript



This is an *Accepted Manuscript*, which has been through the Royal Society of Chemistry peer review process and has been accepted for publication.

Accepted Manuscripts are published online shortly after acceptance, before technical editing, formatting and proof reading. Using this free service, authors can make their results available to the community, in citable form, before we publish the edited article. We will replace this *Accepted Manuscript* with the edited and formatted *Advance Article* as soon as it is available.

You can find more information about *Accepted Manuscripts* in the [Information for Authors](#).

Please note that technical editing may introduce minor changes to the text and/or graphics, which may alter content. The journal's standard [Terms & Conditions](#) and the [Ethical guidelines](#) still apply. In no event shall the Royal Society of Chemistry be held responsible for any errors or omissions in this *Accepted Manuscript* or any consequences arising from the use of any information it contains.

The high thermopower of the Zintl compound $\text{Sr}_5\text{Sn}_2\text{As}_6$ over a wide temperature range: first-principles calculations

Dong Bao Luo, Yuan Xu Wang*, Yu Li Yan, Gui Yang, and Jue Ming Yang

*Institute for Computational Materials Science,
School of Physics and Electronics, Henan University,
Kaifeng 475004, People's Republic of China*

(Dated: June 25, 2014)

Abstract

The thermoelectric properties and the electronic structure of $\text{Sr}_5\text{Sn}_2\text{As}_6$ were studied according to the first principles and semi-classical Boltzmann theory. To elucidate the thermoelectric performance of $\text{Sr}_5\text{Sn}_2\text{As}_6$, we simulated its carrier concentration, Seebeck coefficient, and electrical conductivity, and provided an estimated value for the thermoelectric figure of merit ZT . For pure $\text{Sr}_5\text{Sn}_2\text{As}_6$, the largest Seebeck coefficient (S) is $248 \text{ } (\mu\text{V}/\text{K})$ at 500 K, and the minimum S is $202 \text{ } (\mu\text{V}/\text{K})$ at 1200 K. The large Seebeck coefficient over a wide temperature range most likely results from the appropriate band gap (0.55 eV) of $\text{Sr}_5\text{Sn}_2\text{As}_6$. By studying the carrier concentration dependence of the transport properties, the ZT value for p-type doping was found to be ~ 1.4 times that of n-type doping, which is mainly due to the larger effective mass of the valence band. Moreover, for n-type doping, both the Seebeck coefficient and the electrical conductivity along the z -direction are much larger than those along the other directions, due to the large band degeneracy and light band, which results in the highest ZT value of 3.0 along the z -direction, with a carrier concentration of 9.4×10^{19} electrons per cm^3 at 950 K. The highest ZT value for p-type along the z -direction is 1.7, with a carrier concentration of 1.2×10^{20} holes per cm^3 at 950 K. Meanwhile, the minimum lattice thermal conductivity of $\text{Sr}_5\text{Sn}_2\text{As}_6$ is small ($0.47 \text{ W}/\text{mK}$), and is comparable to those of $\text{Ca}_5\text{M}_2\text{Sb}_6$ ($M = \text{Al}, \text{Ga}, \text{In}$). Hence, good thermoelectric performance along the z -direction for n-type $\text{Sr}_5\text{Sn}_2\text{As}_6$ was predicted.

Keywords: $\text{Sr}_5\text{Sn}_2\text{As}_6$; Thermoelectric properties; Electron localization function; Electronic structure

* E-mail: wangyx@henu.edu.cn

I. INTRODUCTION

Mutual energy transformation between electricity and heat can be achieved via the thermoelectric effect [1]. The thermoelectric effect has attracted great attention due to its cleanliness and convenience as an energy source. The thermoelectric performance of a given material is quantified by a non-dimensional thermoelectric figure of merit $ZT = S^2\sigma T/\kappa$, where S , σ , T , and κ are the Seebeck coefficient, electrical conductivity, absolute temperature, and thermal conductivity, respectively [2]. The thermal conductivity κ is a sum of the electronic (κ_e) and lattice (κ_l) contributions. To achieve a high ZT value, a material simultaneously requires a large Seebeck coefficient, a high electrical conductivity, and a low thermal conductivity. However, the transport properties (S , σ , and κ_e) cannot be independently tuned for increasing ZT due to the strong interdependency of each property via the carrier concentration. Consequently, there are two ways to enhance the ZT value: the first way is to increase the thermoelectric power factor ($S^2\sigma$), which is important for thermoelectric performance; the second way is to decrease the lattice thermal conductivity, which is independent of the electronic structure. Thus, an ideal thermoelectric material should exhibit “phonon glass and electron crystal” behavior [3–6].

As promising thermoelectric materials, Zintl phase compounds always exhibit complex structures and narrow band gaps [7]. In such compounds, the elements with greatly different electronegativity form ionic bonds. The degree of the ionic bonding depends on the difference in electronegativity between the cations and the polyanions. Covalent bonding is produced between polyanions. Thus, the combination of covalent bonding and ionic bonding is a typical feature of Zintl phases. The covalent substructures affect the carrier transport, and the cations strongly scatter phonons. Moreover, the cations donate electrons to the anions, which determines the location of the Fermi level, with little impact on the electronic structure near the Fermi level. Consequently, the carrier concentration can be finely adjusted by doping on the cation site. A small band gap is beneficial for thermoelectric transport properties [8]. Previous study of Zintl compounds, for example $\text{Ca}_5\text{Ga}_2\text{As}_6$ [9], $\text{Ca}_5\text{Al}_2\text{Sb}_6$ [10], $\text{Ca}_5\text{Ga}_2\text{Sb}_6$ [11], and $\text{Yb}_{0.2}\text{Co}_4\text{Sb}_{12}\text{-AgSbTe}_2$ [12], indicated that they are good thermoelectric materials. A high ZT value requires a large Seebeck coefficient that can be explained by the formula $ZT = \frac{rS^2}{L}$ ($r = \kappa_e/\kappa$ and L is the Lorentz constant) [13]. Hence, a large Seebeck coefficient over a wide temperature range in a material is ben-

eficial to its thermoelectric application over a wide temperature range. In addition, good thermoelectric performance is generally found in heavily-doped semiconductors with carrier concentrations on the order of 10^{19} to 10^{21} cm^{-3} . For example, the sample of Na-doping Ca_3AlSb_3 [14] exhibited a high ZT value of 0.8, with a carrier concentration 2.5×10^{19} h^+ cm^{-3} at 1050 K.

$\text{Sr}_5\text{Sn}_2\text{As}_6$ has been experimentally synthesized and was found to be a charge-balanced Zintl phase [15]. The charge-balanced feature may lead to a semiconducting property. Moreover, the structural combination of covalent bonding and ionic bonding, large mass contrast between Sn and As (Sr), and the large number of atoms in its primitive unit cell suggest that $\text{Sr}_5\text{Sn}_2\text{As}_6$ may have unique electronic structure and a low lattice thermal conductivity. In addition, the one-dimensional covalent chains along the c -direction may induce a high electrical conductivity along this direction. $\text{Sr}_5\text{Sn}_2\text{As}_6$ and $\text{Ca}_5\text{M}_2\text{Sb}_6$ ($M = \text{Al}, \text{Ga}, \text{In}$) compounds [11] have similar one-dimensional chain structures and topology along c -direction. In $\text{Ca}_5\text{M}_2\text{Sb}_6$ compounds, the adjacent two chains were connected by Sb-Sb dimers. However, the chains in $\text{Sr}_5\text{Sn}_2\text{As}_6$ are discrete, and no As-As bonding exists in this structure. These features motivate our current study of thermoelectric properties of $\text{Sr}_5\text{Sn}_2\text{As}_6$ and comparison with those of $\text{Ca}_5\text{M}_2\text{Sb}_6$. In thermoelectric materials, the transport properties (S , σ , and κ_e) can not be independently tuned for increasing ZT due to the strong interdependency of each property via the carrier concentration. Thus, it is valuable to explore an optimal carrier concentration to realize a high ZT of $\text{Sr}_5\text{Sn}_2\text{As}_6$. In this work, we calculated the electronic structure and thermoelectric properties of $\text{Sr}_5\text{Sn}_2\text{As}_6$. From the temperature dependent transport properties, the large Seebeck coefficient over a wide temperature range suggests that good thermoelectric properties may be realized in $\text{Sr}_5\text{Sn}_2\text{As}_6$ over a wider temperature range compared to those of $\text{Ca}_5\text{M}_2\text{Sb}_6$ ($M = \text{Al}, \text{Ga}, \text{In}$). In addition, the minimum lattice thermal conductivity (κ_{min}) of $\text{Sr}_5\text{Sn}_2\text{As}_6$ is comparable to those of $\text{Ca}_5\text{M}_2\text{Sb}_6$. The ZT value for p-type doping is ~ 1.4 times that of n-type doping, which is due to the heavier valence band. Moreover, for n-type doping, both the Seebeck coefficient and the electrical conductivity along the z -direction are larger than those along other directions, which results in the highest ZT (3.0 at 950 K), with a carrier concentration of 9.4×10^{19} e cm^{-3} . For p-type doping, the highest ZT is 1.7 at 950 K along the z -direction, corresponding to a carrier concentration of 1.2×10^{20} h^+ cm^{-3} . In addition, an effective doping method is to adjust the content of As and Sn atoms in $\text{Sr}_5\text{Sn}_2\text{As}_6$, which can be seen from the spatial

distribution of the electrons and the calculated density of states.

II. COMPUTATIONAL DETAIL

The Vienna Ab-initio Simulation Package (VASP) [16] based on the Projector augmented wave (PAW) method [17] was used to optimize the geometry. We used the generalized-gradient approximation (GGA), as parameterized by Perdew, Burke, and Ernzerhof to describe the exchange-correlation function [18]. The plane-wave cutoff energy was 450 eV, and the energy convergence criterion was chosen to be 10^{-6} eV. The Hellmann-Feynman forces on each ion were less than 0.02 eV/Å, and the Brillouin zones of the unit cells were represented by the Monkhorst-Pack special k-point scheme using $3 \times 3 \times 9$ grid meshes.

The electronic structures of $\text{Sr}_5\text{Sn}_2\text{As}_6$ were calculated by the full potential-linearized augmented plane wave (FP-LAPW) methods [19] based on the density functional theory (DFT) [20, 21]. The modified Becke-Johnson (MBJ) [22, 23] semi-local exchange potential was used to improve the accuracy of the band gap, as implemented in the WIEN2k [24–26]. The muffin-tin radii were 2.50 a.u. for Sr, Sn, and As. The cutoff parameter is $R_{mt} \times K_{max} = 7$ (K_{max} is the magnitude of the largest k vector), and the number of k points of the self-consistent calculations was 1000 in the Brillouin zone. The thermoelectric transport properties were calculated through the semi-classical Boltzmann theory and the rigid-band approach, which is implemented in the BoltzTrap code [27]. With the Boltzmann theory, the constant scattering time approximation was used. This approximation, which is commonly applied for metals and degenerately doped semiconductors, is based on the assumption that the scattering time determining the electrical conductivity does not vary strongly with energy on the scale of $k_B T$. This approximation does not involve any assumption about the possibly strong doping and temperature dependence of τ . In this way, the Seebeck coefficient S is independent of the relaxation time (τ), while the electrical conductivity σ and κ_e can only be evaluated with respect to the parameter τ .

III. RESULTS AND DISCUSSION

A. Structure and stability

The $\text{Sr}_5\text{Sn}_2\text{As}_6$ compound belongs to the $\text{Sr}_5\text{Sn}_2\text{P}_6$ type, and it is orthorhombic with the space group of $Pbam$. The primitive cell of $\text{Sr}_5\text{Sn}_2\text{As}_6$ contains 26 atoms. For $\text{Sr}_5\text{Sn}_2\text{As}_6$, the calculated lattice constants are $a = 12.6847 \text{ \AA}$, $b = 14.1802 \text{ \AA}$, and $c = 4.3121 \text{ \AA}$, which are close to the reported experimentally measured value [15]. Fig. 1(a) shows the optimized crystal structure of $\text{Sr}_5\text{Sn}_2\text{As}_6$, which exhibits high symmetry and large anisotropy. The right panel is the corresponding first Brillouin zone shape (from the primitive unit cell). The As atoms have three non-equivalent positions, labeled as As1, As2, and As3. The Sr atoms also have three non-equivalent positions, labeled as Sr1, Sr2, and Sr3. As seen from Fig. 1, $\text{Sr}_5\text{Sn}_2\text{As}_6$ is composed of infinite chains of corner-shared SnAs_4 tetrahedra along the c -axis, and these chains are separated by Sr atoms. The structure along the c -axis is different from that along the a - and b -axes, which may induce the anisotropy of thermoelectric properties. The high anisotropy of the lattice structure for $\text{Sr}_5\text{Sn}_2\text{As}_6$ is likely to exhibit a large difference in the thermoelectric properties along the different directions. For example, for SnSe, which has a layered structure, the high ZT value of 2.6 along the b -direction and 2.3 along the c -direction are ~ 3 times that of ZT value of 0.8 along the a -direction [28].

To verify the stability of orthorhombic $\text{Sr}_5\text{Sn}_2\text{As}_6$, we calculated the phonon frequency and the formation energy. The phonon dispersion curves in the orthorhombic Brillouin zone were calculated and are shown in Fig. 2. As seen from this figure, there is no imaginary phonon frequency at any of the wave vectors, indicating the dynamical stability of orthorhombic $\text{Sr}_5\text{Sn}_2\text{As}_6$. The formation energy is a more direct evidence of the stability of a material, which can be estimated from the following:

$$\Delta E = E_{(\text{Sr}_5\text{Sn}_2\text{As}_6)} - 5E_{(\text{Sr})} - 2E_{(\text{Sn})} - 6E_{(\text{As})}, \quad (1)$$

where $E_{(\text{Sr}_5\text{Sn}_2\text{As}_6)}$ is the total energy of $\text{Sr}_5\text{Sn}_2\text{As}_6$ at its most stable phase. $E_{(\text{Sr})}$, $E_{(\text{Sn})}$, and $E_{(\text{As})}$ are the total energy per atom of Sr (space group: $Fm\bar{3}m$), Sn (space group: $Cmmm$), and As (space group: $R\bar{3}m$) in their bulk phases, respectively. The calculated formation energy is -11.9 eV, which means that $\text{Sr}_5\text{Sn}_2\text{As}_6$ is stable. As seen from Fig. 2, the soft acoustic and optic vibration modes in $\text{Sr}_5\text{Sn}_2\text{As}_6$ reflect its low lattice thermal conductivity.

B. Elastic and thermal properties

To further check the mechanical stability of orthorhombic $\text{Sr}_5\text{Sn}_2\text{As}_6$, we also calculated the elastic constants. The strain-stress method was used to obtain their elastic constants. A small finite strain was applied on the optimized structure, and then the atomic positions were optimized. Next, the elastic constants were obtained from the stress of the strained structure and the strains. Below is the matrix of the elastic constants (in GPa) of orthorhombic $\text{Sr}_5\text{Sn}_2\text{As}_6$,

$$c_{ij} = \begin{pmatrix} 68 & 27 & 16 & 0 & 0 & 0 \\ 27 & 68 & 24 & 0 & 0 & 0 \\ 16 & 24 & 81 & 0 & 0 & 0 \\ 0 & 0 & 0 & 19 & 0 & 0 \\ 0 & 0 & 0 & 0 & 14 & 0 \\ 0 & 0 & 0 & 0 & 0 & 30 \end{pmatrix}. \quad (2)$$

We calculated the eigenvalues of the elastic constant matrix and found that all eigenvalues are positive, which indicates that the orthorhombic $\text{Sr}_5\text{Sn}_2\text{As}_6$ is elastically stable. Additionally, we acquired its bulk modulus $K = 39$ GPa and shear modulus $G = 23$ GPa from the calculated elastic constants, which can further generate the minimum lattice thermal conductivity (κ_{min}) through the discussion below.

As mentioned above, the total thermal conductivity (κ) in a typical thermoelectric material is the sum of electronic (κ_e) and lattice (κ_l) contributions. The lattice thermal conductivity follows the $1/T$ dependence when the phonon transport is dominated by Umklapp scattering above the Debye temperature (Θ_D). However, this process continues until the minimum lattice thermal conductivity (κ_{min}) is reached. κ_{min} can be approximated at high temperature ($T > \Theta_D = 312$ K) by

$$\kappa_{min} = \frac{1}{2} \left(\frac{\pi}{6} \right)^{1/3} k_B V^{-2/3} (2\nu_s + \nu_l), \quad (3)$$

$$\nu_s = \sqrt{\frac{G}{d}}, \quad (4)$$

$$\nu_l = \sqrt{\frac{K + \frac{4}{3}G}{d}}, \quad (5)$$

where V is the average volume of per atom, ν_s and ν_l are the longitudinal and shear sound velocities, respectively, and d is the theoretical density [29]. As shown in Fig. 1, the primitive

unit cell of $\text{Sr}_5\text{Sn}_2\text{As}_6$ contains 26 atoms. Such a large number of atoms in the primitive unit cell can result in a low lattice thermal conductivity due to the low velocity of the optical modes. Moreover, the high mass contrast between Sn and As (Sr) is also helpful to decrease the lattice thermal conductivity of $\text{Sr}_5\text{Sn}_2\text{As}_6$, which is associated with the flattening of the optical modes for higher mass contrast [30]. As shown in Table I, the relatively high density and the low stiffness of $\text{Sr}_5\text{Sn}_2\text{As}_6$ decreases the sound velocity and hence decreases its lattice thermal conductivity. Further decreasing the lattice thermal conductivity can be achieved by increasing disorder, nanostructure, doping with heavy elements, etc. Because κ_l is larger than κ_{min} , the improvements in $\text{Sr}_5\text{Sn}_2\text{As}_6$ can be achieved by reducing κ_{min} , which can be achieved by reducing the speed of sound from Eq. (3). As can be seen from Table I, the order of shear moduli (G), bulk moduli (K), longitudinal velocity (ν_s), and shear sound velocity (ν_l) are $\text{Ca}_5\text{Al}_2\text{Sb}_6 > \text{Ca}_5\text{Ga}_2\text{Sb}_6 > \text{Sr}_5\text{Sn}_2\text{As}_6 > \text{Ca}_5\text{In}_2\text{Sb}_6$, and the minimum lattice thermal conductivities (κ_{min}) of these compounds are in reverse order. The κ_{min} of $\text{Sr}_5\text{Sn}_2\text{As}_6$ (0.47 W/mK) is comparable to that of $\text{Ca}_5\text{Al}_2\text{Sb}_6$ (0.53 W/mK), $\text{Ca}_5\text{Ga}_2\text{Sb}_6$ (0.50 W/mK), and $\text{Ca}_5\text{In}_2\text{Sb}_6$ (0.46 W/mK). As $\text{Ca}_5\text{M}_2\text{Sb}_6$ ($M = \text{Al, Ga, Sb}$) exhibit low thermal conductivities, $\text{Sr}_5\text{Sn}_2\text{As}_6$ is expected to exhibit a low thermal conductivity. The order of the general atomic masses is $\text{Ca}_5\text{Al}_2\text{Sb}_6 < \text{Ca}_5\text{Ga}_2\text{Sb}_6 < \text{Sr}_5\text{Sn}_2\text{As}_6 < \text{Ca}_5\text{In}_2\text{Sb}_6$, which confirms that the cause of the lattice stiffness reduction is that heavier atoms possess orbitals that are more diffuse, leading to a lower degree of electron density overlap with the neighboring atoms [11]. Hence, doping with heavier elements in $\text{Sr}_5\text{Sn}_2\text{As}_6$ may lead to a lower lattice thermal conductivity.

C. Electrical transport properties

As previously mentioned, a good thermoelectric material requires a large Seebeck coefficient and a high electrical conductivity. For metals or degenerate semiconductors (parabolic band, energy-independent scattering approximation), the Seebeck coefficient is defined as Eq. (6) [31]. The electrical conductivity is given by Eq. (7). The carriers mobility is strongly affected by the band mass of a single valley, as can be seen from Eq. (8).

$$S = \frac{8\pi^2 k_B^2}{3eh^2} m^* T \left(\frac{\pi}{3n}\right)^{2/3}, \quad (6)$$

$$\sigma = ne\eta = \frac{1}{\rho}, \quad (7)$$

$$\eta \propto \frac{1}{m_b^*}, \quad (8)$$

here, k_B is the Boltzmann constant, h is the Planck constant, m^* is the density-of-states effective mass, m_b^* is the band mass of a single valley, T is the absolute temperature, and n is carrier concentration. From Eq. (6), we can see that S is proportional to temperature and to the density-of-states effective mass, and it is inversely proportional to the carrier concentration. The value of σ is proportional to the carrier concentration and varies inversely with the density-of-states effective mass. Hence, we studied the thermoelectric performance as a function of temperature and carrier concentration to achieve a good balance between S and σ . The temperature and carrier concentration dependence of n , S , $\frac{\sigma}{\tau}$, and $\frac{S^2\sigma}{\tau}$ were calculated using the semi-classical Boltzmann theory and the rigid-band approach. To estimate a rough value of ZT of $\text{Sr}_5\text{Sn}_2\text{As}_6$, we used the relaxation time of $\text{Ca}_5\text{Al}_2\text{Sb}_6$ to simulate its transport properties because they have similar crystal structures.

Fig. 3(a) shows that the carrier concentration of $\text{Sr}_5\text{Sn}_2\text{As}_6$ increases with the increase of temperature, which indicates that the thermal excitation becomes strong, which causes the increase of the intrinsic carrier concentration. As seen in Fig. 3(b), the S value is positive over the entire studied temperature range, indicating a p-type transport for $\text{Sr}_5\text{Sn}_2\text{As}_6$. S increases with the increase in temperature, which results in the largest value at 500 K, followed by a decrease. The maximum S is 248 ($\mu\text{V}/\text{K}$) at 500 K, which is much larger than that of $\text{Ca}_5\text{Ga}_2\text{As}_6$ (200 $\mu\text{V}/\text{K}$ at 850 K) [9]. In addition, the minimum S is 202 ($\mu\text{V}/\text{K}$) at 1200 K. The large S value over a wide temperature range is beneficial for thermoelectric applications, as explained by the formula $ZT = \frac{rS^2}{L}$ ($r = \kappa_e/\kappa$ and L is the Lorentz constant), which indicates that it is impossible to have a high and stable ZT value without a high and stable S [13]. Hence, good thermoelectric performance may be realized in $\text{Sr}_5\text{Sn}_2\text{As}_6$ over a wide temperature range. Thus, $\text{Sr}_5\text{Sn}_2\text{As}_6$ is a promising thermoelectric material because the S value is large over a wide temperature range compared with the experimental S value of other known good thermoelectric materials of $\text{Ca}_5\text{M}_2\text{Sb}_6$ ($M = \text{Al}, \text{Ga}, \text{In}$), with a similar structure to that shown in Fig. 4(a). From Eq. (6), $S = a \times (\frac{1}{n})^{2/3}$, where $a = \frac{8\pi^2 k_B^2}{3eh^2} m^* T (\frac{\pi}{3})^{2/3}$. The amount of change of S value is related to n at the same temperature. As a result, the high S over a wide range temperature for $\text{Sr}_5\text{Sn}_2\text{As}_6$ is due to the smaller amount of change in n compared with that of $\text{Ca}_5\text{M}_2\text{Sb}_6$ ($M = \text{Al}, \text{Ga}, \text{In}$) at the same temperature. Moreover, the large S over the wide temperature range may result

from the larger band gap (0.55 eV) than that of $\text{Ca}_5\text{M}_2\text{Sb}_6$ ($M = \text{Al}, \text{Ga}, \text{In}$) [11]. From Fig. 3(c), σ decreases with the increasing temperature, which means that the mobility of carriers decreases due to the increased phonon scattering. Further, we can calculate an estimated thermoelectric figure of merit $ZT = \frac{S^2 \cdot \frac{\sigma}{\tau} \cdot \tau \cdot T}{\kappa_{min}}$, where $\tau = 8.68 \times 10^{-6} T^{-1} n^{-1/3}$ is the relaxation time of $\text{Ca}_5\text{Al}_2\text{Sb}_6$ [32]; because κ_e is usually much smaller than κ_l , it is ignored here. The figure of merit can assess the thermoelectric properties of $\text{Sr}_5\text{Sn}_2\text{As}_6$ to some extent. From Fig. 3(d), the maximum ZT value is 1.0 at 800 K, which is comparable to the known good thermoelectric materials, such as PbTe [33].

As seen in Fig. 3, pure $\text{Sr}_5\text{Sn}_2\text{As}_6$ was expected to be a promising thermoelectric material at high temperature. However, the carrier concentration of pure $\text{Sr}_5\text{Sn}_2\text{As}_6$ is relatively low, and its potential as a good thermoelectric material is not fully realized. The transport properties (S , σ , and κ_e) can not be independently tuned for increasing ZT due to the strong correlation of each property via the carrier concentration. Therefore, the primary conventional effort for maximizing ZT of $\text{Sr}_5\text{Sn}_2\text{As}_6$ is to find an optimal carrier concentration. For example, Zn and Na doping can improve the thermoelectric performance of $\text{Ca}_5\text{Al}_2\text{Sb}_6$ [34, 35]. As shown in Fig. 4(b), the Seebeck coefficient of $\text{Sr}_5\text{Sn}_2\text{As}_6$, with p-type doping, is larger than that of $\text{Ca}_5\text{M}_2\text{Sb}_6$ ($M = \text{Al}, \text{Ga}, \text{In}$) in the experimental part at 700 K, which indicates that $\text{Sr}_5\text{Sn}_2\text{As}_6$ may achieve a better thermoelectric performance by p-type doping [33]. The combined Seebeck coefficient is given [36] by

$$S = \frac{S_e \sigma_e + S_h \sigma_h}{\sigma_e + \sigma_h}, \quad (9)$$

$$S_h = \frac{\kappa_B}{e} \left[\ln\left(\frac{N_v}{p}\right) + 2.5 - \gamma \right], \quad (10)$$

$$S_e = -\frac{\kappa_B}{e} \left[\ln\left(\frac{N_c}{n}\right) + 2.5 - \gamma \right], \quad (11)$$

where γ is the scattering mechanism parameter, S_h (S_e) is the Seebeck coefficient of holes (electrons), σ_e (σ_h) is the electrical conductivity of electrons (holes), N_v (N_c) is the effective density of states in the valence band (conduction band), n is the number of electrons, and p is the number of holes. The carrier concentration dependences of the thermoelectric transport properties were calculated and plotted in Fig. 5. As can be seen from Fig. 5(a), the Seebeck coefficient of p-type $\text{Sr}_5\text{Sn}_2\text{As}_6$ is positive, while that of n-type is negative, which are in agreement with Eq. (10) and Eq. (11), respectively. The absolute value of the Seebeck

coefficient for p-type is larger than that for n-type, due to its larger effective mass of the valence band shown in the calculated band structure. Meanwhile, bipolar reduction in the thermopower can be seen for p-type from 950 K to 1100 K. There is also a bipolar effect for n-type $\text{Sr}_5\text{Sn}_2\text{As}_6$, when the carrier concentration is below $4.8 \times 10^{19} \text{ cm}^{-3}$. As is known, the bipolar effect is a consequence of a small band gap that gives rise to two types of carriers participating in transportation corresponding to Eq. (12), which is unfavorable for thermoelectric performance. Hence, to obtain a large Seebeck coefficient, it is worth seeking for ways to reduce the bipolar effect. From Fig. 5(b), the electrical conductivity increases with the increase of the carrier concentration, which is consistent with Eq. (7). However, the electrical conductivity decreases from 500 K to 950 K, and eventually to 1100 K, which is mainly caused by the increased phonon scattering with the increase of temperature. The electrical conductivity of the n-type $\text{Sr}_5\text{Sn}_2\text{As}_6$ is larger than that of the p-type one, due to its smaller conduction-band effective mass. As can be seen in Fig. 5(c), the calculated ZT value of the p-type $\text{Sr}_5\text{Sn}_2\text{As}_6$ is larger than that of n-type $\text{Sr}_5\text{Sn}_2\text{As}_6$ because the value of n is below $1 \times 10^{21} \text{ cm}^{-3}$. Above this carrier concentration, the calculated ZT value of the p-type $\text{Sr}_5\text{Sn}_2\text{As}_6$ is smaller than that of the n-type one. Moreover, the high ZT over the entire studied carrier concentration range appears for p-type doping of $\text{Sr}_5\text{Sn}_2\text{As}_6$ at the same temperature, due to the large Seebeck coefficient of the p-type $\text{Sr}_5\text{Sn}_2\text{As}_6$ shown in Fig. 5(a).

To investigate the most favorable direction for thermoelectric application in $\text{Sr}_5\text{Sn}_2\text{As}_6$, we also calculated the transport properties as a function of carrier concentration from $1 \times 10^{19} \text{ cm}^{-3}$ to $1 \times 10^{21} \text{ cm}^{-3}$ along the x -, y -, and z -directions at 950 K. For the p-type $\text{Sr}_5\text{Sn}_2\text{As}_6$ shown in Figs. 6(a) and 6(b), the Seebeck coefficient along the x -direction is larger than those along other two directions, due to its larger band effective mass along the x -direction shown in the calculated band structure. The electrical conductivity along the z -direction is larger than those along other two directions, due to the smaller band effective mass along the z -direction. However, for n-type $\text{Sr}_5\text{Sn}_2\text{As}_6$, both the Seebeck coefficient and the electrical conductivity along the z -direction are larger than those along the other two directions. This difference is most likely due to the larger degeneracy and lighter band along $\Gamma - Z$ than those along $\Gamma - X$ and $\Gamma - Y$, as shown in Fig. 8, which may induce a larger Seebeck coefficient and a higher electrical conductivity along the z -direction than those along the other directions. From Fig. 6(c), ZT along the z -direction for p-type and

n-type doping are both larger than that along the x - and y -directions. Moreover, ZT of the n-type $\text{Sr}_5\text{Sn}_2\text{As}_6$ along the z -direction is larger than that of p-type doping in the three orthogonal directions. The maximum ZT of n-type $\text{Sr}_5\text{Sn}_2\text{As}_6$ is 3.0 along the z -direction at 950 K, corresponding to a carrier concentration of $9.4 \times 10^{19} \text{ e cm}^{-3}$, which is mainly due to the lack of conflict between S and σ . For p-type doping, the maximum ZT is 1.7 along the z -direction at the same temperature, with a carrier concentration of $1.2 \times 10^{20} \text{ h}^+ \text{ cm}^{-3}$. Therefore, good thermoelectric performance along the z -direction for n-type $\text{Sr}_5\text{Sn}_2\text{As}_6$ is predicted.

D. Electronic structure

The electronic structure is crucial for the interpretation of the transport properties. The electronic distribution, band dispersion, valley degeneracy, and band gap play important roles in the transport properties. Hence, we calculated the electron localization function (ELF), band structure, band decomposed charge density, and density of states (DOS). The electronegativity values are similar for the atoms of covalent bonding, but an ionic bonding regularly arises due to the different electronegativity values for the $\text{A}_5\text{M}_2\text{Pn}_6$ compounds. For $\text{Sr}_5\text{Sn}_2\text{As}_6$, the electronegativity values are 0.95, 1.96, and 2.18 for Sr, Sn, and As, respectively. The Sn and As atoms tend to form covalent bonds, and the Sr atom tends to form ionic bonds. To clearly demonstrate the bonding character, we calculated the electron localization function (ELF), which can describe the characterization of the localized electron distribution [37]. According to the definition of ELF, the value of ELF ranges from 0 to 1. $\text{ELF} = 1$ indicates completely localized electrons, and $\text{ELF} = 0$ indicates completely delocalized electrons, and $\text{ELF} = 0.5$ indicates that the electrons form electron-gas-like pairs that can transfer electrons easily. From Fig. 7, we can clearly see the chemical bonding character in $\text{Sr}_5\text{Sn}_2\text{As}_6$. The right panel is the ELF isosurface that shows the region of charge accumulation, which can identify covalent bonding in the entire cellular space. A certain degree of charge accumulation occurs midway between Sn and As atoms, suggesting that these bonds have significant covalent character. The more diffuse regions of charge between As and Sr atoms indicate ionic bonding character. To investigate the infinite, one-dimensional, ladder-like moieties qualitatively, we plotted the two-dimensional charge density in a supercell along the z -direction. For the left pattern, high ELF value

(0.92) of the blue area indicates the highly localized electrons. The red area is close to 0, indicating that the electrons of this area are highly delocalized. The ELF value of the area between Sn and As is approximately 0.78, which indicates a strong covalent bonding between them. It is known that the electron density of ionic bonding is localized around the atoms. The ELF value of the area around the As atom close to the Sr atom is approximately 0.89, and the ELF value of the area around the Sr atom is approximately 0.90, indicating an ionic bonding feature. From the chains of the corner-shared SnAs_4 tetrahedron along the z -axis, we found that there exists an electronic channel along the As-Sn-As covalent chains, which can easily transport electrons. $\text{Sr}_5\text{Sn}_2\text{As}_6$ is composed of infinite chains of corner-shared SnAs_4 tetrahedron along the z -axis, so that larger electronic conductivity along the z -axis compared to that along the x - and y -axes can be understood.

We know that the transport properties are closely related to the electronic states near the conduction band minimum (CBM) and the valence band maximum (VBM). Hence, we focus our discussions on the electronic states near the Fermi level [38]. As seen from the calculated band structure shown in Fig. 8, $\text{Sr}_5\text{Sn}_2\text{As}_6$ is a semiconductor with an indirect gap of 0.55 eV. The CBM and the VBM are located at the Γ and Y points, respectively. Moreover, the dispersion along the $\Gamma - Z$ direction is greater than that along the $\Gamma - X$ direction, which induces the larger electrical conductivity of the n-type $\text{Sr}_5\text{Sn}_2\text{As}_6$ than that of the p-type $\text{Sr}_5\text{Sn}_2\text{As}_6$. For a qualitative description, the band effective mass is given by

$$m^* = \hbar^2 \left[\frac{d^2 E(K)}{dk^2} \right]_{E(k)=E_f}^{-1} \quad (12)$$

The calculated band effective masses are $m_x^* = 0.34 m_e$ (along $\Gamma - X$), $m_y^* = 0.27 m_e$ (along $\Gamma - Y$), and $m_z^* = 0.08 m_e$ (along $\Gamma - Z$) for the conduction band. For the valence band, m_x^* , m_y^* , and m_z^* are $-1.64 m_e$, $-0.78 m_e$, and $-0.11 m_e$, respectively. As is well known, light bands are beneficial for large electrical conductivity, while bands of heavy and large degeneracy can produce high Seebeck coefficients. Therefore, it is easy to understand the anisotropy of the transport properties shown in Fig. 6. The mixture of light and heavy bands near the Fermi level is conducive to obtaining good thermoelectric properties, similar to $\text{Ca}_5\text{M}_2\text{Sb}_6$ ($M = \text{Al}, \text{Ga}, \text{In}$) [11] and $\text{Ca}_5\text{Ga}_2\text{As}_6$ [9]. The m_{DOS}^* was calculated by

$$m_{DOS}^* = (m_1^* m_2^* m_3^*)^{1/3} N_v^{2/3}, \quad (13)$$

where m_1^* , m_2^* , m_3^* are the effective mass components along three perpendicular directions, and N_v is the band degeneracy. The calculated m_{DOS}^* of electrons ($0.31 m_e$) is much smaller

than the absolute value of the effective mass of holes ($-0.83 m_e$), which further proves that the Seebeck coefficient of p-type doping is higher than that of n-type doping, but the p-type doping electrical conductivity is smaller than that of n-type doping, which is consistent with Fig. 5. The calculated band decomposed charge density for conduction band valleys near the Fermi level at the Γ point and the valence band valleys near the Fermi level at the Y point were plotted in Fig. 9. Fig. 9(a) shows that CBM mainly consists of the electrons around the As1-Sn-As1 chains. However, for the VBM shown in Fig. 9(b), it is composed of electrons around As atoms in the following order: $As_2 > As_3 > As_1$. This calculation proved that the transport properties are mainly affected by As1 and Sn atoms for n-type doping, while they are mainly affected by As2, As3, and As1 atoms for p-type doping; these observations can provide guidance for further investigating the doping effect on $Sr_5Sn_2As_6$ with the appropriate atoms.

To clearly observe the states near the Fermi level, we calculated the DOS, as shown in Fig. 10. In principle, a broad DOS means a strong electronic delocalization; a sharp DOS corresponds to a strong electronic localization. Fig. 10(b) confirms that the valence band edge is mainly composed of As2, As3, and As1 atoms, and the conduction band edge mainly consists of Sn and As1 atoms, which agrees well with the results in Fig. 9. The hybridized DOS of the Sn and As1 atoms indicates a covalent bonding character, which is beneficial to electrical transport. Fig. 10(c) shows our calculated partial density of states (PDOS) of the Sr1, As1, and Sn atoms. The bonding feature for the Sn s - and the As1 p -orbit can be seen the states from -5.5 eV to -6.8 eV, and the anti-bonding feature can be seen from -0.5 eV to 2 eV, which is consistent with the covalent bonding feature between the Sn and As atoms shown in Fig. 7. The valence band near the Fermi level is composed primarily of the As1 p -orbit. The Sn p -orbit and the As1 p -orbit are strongly hybridized from -2 eV to -3.5 eV. Hence, an effective doping approach involves replacing As and Sn sites for accurately adjusting the carrier concentrations.

IV. CONCLUSION

In summary, first-principle calculations and the semi-classical Boltzmann theory were used to study the electronic and thermoelectric properties of $Sr_5Sn_2As_6$. It is found that the transport properties of p-type $Sr_5Sn_2As_6$ are most likely better than those of n-type doping,

which is mainly due to the heavier valence band. The light band mass along the $\Gamma - Z$ direction induced a high conductivity of n-type $\text{Sr}_5\text{Sn}_2\text{As}_6$ along the z -direction. Moreover, n-type $\text{Sr}_5\text{Sn}_2\text{As}_6$ along the z -direction has a large Seebeck coefficient simultaneously at 950 K, which is most likely due to the large band degeneracy along the z -direction. The highest ZT value is 3.0 for n-type doping along the z -direction at 950 K, corresponding to a carrier concentration of $9.4 \times 10^{19} \text{ e cm}^{-3}$. For p-type doping, the highest ZT is 1.7 along the z -direction at 950 K, with a carrier concentration of $1.2 \times 10^{20} \text{ h}^+ \text{ cm}^{-3}$. The spatial distribution of the electrons and the DOS calculations can provide guidance for doping in $\text{Sr}_5\text{Sn}_2\text{As}_6$. In addition, the minimum lattice thermal conductivity of $\text{Sr}_5\text{Sn}_2\text{As}_6$ is expected to be small (0.47 W/mK) due to its complex structure. Hence, it is clearly possible to obtain good thermoelectric performance along the z -direction for n-type $\text{Sr}_5\text{Sn}_2\text{As}_6$.

V. ACKNOWLEDGMENTS

This research was sponsored by the National Natural Science Foundation of China (Nos. 21071045, 51371076, and U1204112), the Program for Innovative Research Team (in Science and Technology) in University of Henan Province (No. 13IRTSTHN017).

VI. REFERENCES

-
- [1] D. T. Crane and J. W. LaGrandeur, *J. Electron. Mater.*, 2000, **39**, 2142.
 - [2] G. Mahan, B. Sales, and J. Sharp, *Phys. Today*, 1997, **50**, 42.
 - [3] A. F. Ioffe, *Physics of Semiconductors* (Academic Press, New York, 1960).
 - [4] D. M. Rome, *CRC Handbook of Thermoelectric* (CRC Press, Boca Raton, FL, 1995).
 - [5] T. M. Tritt, *Science*, 1999, **283**, 804.
 - [6] F. J. DiSalvo, *Science*, 1999, **285**, 703.
 - [7] S. M. Kauzlarich, S. R. Brown and G. J. Snyder, *Dalton Trans.*, 2007, **21**, 2099.
 - [8] F. Gascoin, S. Ottensmann, D. Stark, S. M. Haile and G. J. Snyder, *Adv. Funct. Mater.*, 2010, **20**, 4375.
 - [9] Y. L. Yan, Y. X. Wang, and G. B. Zhang, *J. Mater. Chem.*, 2012, **22**, 20284-20290.

- [10] Y. L. Yan and Y. X. Wang, *J. Mater. Chem.*, 2011, **21**, 12497-12502.
- [11] A. Zevalkink, G. S. Pomrehn, S. Johnson, *Chem. Mater.*, 2012, **24**, 2091-2098.
- [12] J. Y. Peng, L. W. Fu, Q. Z. Liu, M. Liu, J. Y. Yang, D. Hitchcock, M. H. Zhou and J. He, *J. Mater. Chem. A*, 2014, **2**, 73-79.
- [13] D. J. Singh and D. Parker, *J. Appl. Phys.*, 2013, **114**, 143703.
- [14] A. Zevalkink, E. S. Toberer, W. G. Zeier, E. Flage-Larsen and G. J. Snyder, *Energy Environ. Sci.*, 2011, **4**, 510-518.
- [15] J. Wang, S. Q. Xia, and X. T. Tao, *Inorg. Chem.*, 2012, **51**, 5771-5778.
- [16] G. Kresse and J. Hafner, *J. Phys.: Condens. Matter*, 1994, **6**, 8245.
- [17] P. E. Blochl, *Phys. Rev. B*, 1994, **50**, 17953.
- [18] D. M. Ceperley and B. J. Alder, *Phys. Rev. Lett.*, 1980, **45**, 566.
- [19] D. Singh, *Planewaves, Pseudopotentials, and the LAPW Method* (Kluwer Academic, Boston, MA, 1994).
- [20] L. H. Thomas, *Proc. Cambridge Philos. Soc.*, 1927, **23**, 542.
- [21] E. Fermi, *Z. Phys.*, 1928, **48**, 73.
- [22] F. Tran and P. Blaha, *Phys. Rev. Lett.*, 2009, **102**, 226401.
- [23] E. Engel and S.H. Vosko, *Phys. Rev. B*, 1993, **47**, 13164.
- [24] D. D. Koelling and B. N. Harmon, *J. Phys. C*, 1997, **10**, 3107.
- [25] P. Hohenberg and W. Kohn, *Phys. Rev.*, 1964, **136**, B864.
- [26] P. Blaha, K. Schwarz, G. K. H. Madsen, D. Kvasnicka, and J. Luitz: *WIEN2K. An Augmented Plane Wave + Local Orbitals Program for Calculating Crystal Properties* (Vienna Univ. Technology, Vienna, 2001).
- [27] G. K. H. Madsen and D. J. Singh, *Comput. Phys. Commun.*, 2006, **175**, 67.
- [28] L. D. Zhao, S. H. Lo, Y. S. Zhang, H. Sun, C. Uher, C. Wolverton, V. P. Dravid, and M. G. Kanatzidis, *Nature*, 2014, **508**, 373-377.
- [29] D. G. Cahill, S. K. Watson, R. O. Pohl, *Phys. Rev. B*, 1992, **46**, 6131.
- [30] E. S. Tober, A. Zevalkink, and G. J. Snyder, *J. Mater. Chem.*, 2011, **21**, 15843-25852.
- [31] M. Cutler, J. F. Leavy, and R. L. Fitzpatrick, *Phys. Rev.*, 1964, **133**, A1143.
- [32] K. P. Ong, D. J. Singh, P. Wu, *Phys. Rev. B*, 2011, **83**, 115110.
- [33] Y. X. Wang, X. Chen, T. Cui, Y. L. Niu, Y. C. Wang, M. Wang, Y. M. Ma and G. T. Zou, *Phys. Rev. B*, 2007, **76**, 155127.

- [34] A. Zevalkink, E. S. Toberer, T. Bleith, et al., *J. Appl. Phys.*, 2011, **110**, 013721.
- [35] E. S. Toberer, A. Zevalkink, N. Crisosto, et al., *Adv. Funct. Mater.*, 2010, **20**, 4375-4380.
- [36] M. C. Chen, *J. Appl. Phys.*, 1992, **71**, 3636.
- [37] A. Savin, R. Nesper, S. Wengert, et al., *Angew. Chem. Int. Ed.*, 1997, **36**, 1808-1832.
- [38] S. G. Louie, and M. L. Cohen, *Phys. Rev. B*, 1976, **13**, 2461.

FIGURE CAPTIONS

- Fig. 1. (a) The optimized crystal structure of $\text{Sr}_5\text{Sn}_2\text{As}_6$. Magenta, red, and green spheres represent Sr, As, and Sn atoms, respectively; (b) The first Brillouin zone (from the primitive unit cell) of $\text{Sr}_5\text{Sn}_2\text{As}_6$.
- Fig. 2. Phonon dispersion curves of $\text{Sr}_5\text{Sn}_2\text{As}_6$.
- Fig. 3. Calculated thermoelectric properties of $\text{Sr}_5\text{Sn}_2\text{As}_6$ as a function of temperature.
- Fig. 4. Seebeck coefficient of $\text{Ca}_5\text{M}_2\text{Sb}_6$ ($M = \text{Al}, \text{Ga}, \text{In}$) in experimental part and $\text{Sr}_5\text{Sn}_2\text{As}_6$ in theory as a function of (a) temperature and (b) carrier concentration at 700 K, respectively. S (unit in $(\mu\text{V}/\text{K})$).
- Fig. 5. The calculated thermoelectric properties of p -type and n -type $\text{Sr}_5\text{Sn}_2\text{As}_6$ as a function of carrier concentration from 1×10^{19} to $6 \times 10^{21} \text{ cm}^{-3}$ at 500 K, 950 K, and 1100 K.
- Fig. 6. The thermoelectric anisotropy of $\text{Sr}_5\text{Sn}_2\text{As}_6$ as a function of carrier concentration from 1×10^{19} to $1 \times 10^{21} \text{ cm}^{-3}$ at 950 K.
- Fig. 7. Calculated electron localization function of $\text{Sr}_5\text{Sn}_2\text{As}_6$ for the (100) plane (left) and the whole unit cell (right) with the isosurface value of 0.78.
- Fig. 8. Calculated band structure of $\text{Sr}_5\text{Sn}_2\text{As}_6$.
- Fig. 9. Band decomposed charge density of (a) conductive bands near the Fermi level at Γ point and (b) valence bands near the Fermi level at Y point for $\text{Sr}_5\text{Sn}_2\text{As}_6$ with the isosurface value of 0.0035.
- Fig. 10. Calculated projected density-of-states for (a) $\text{Sr}_5\text{Sn}_2\text{As}_6$; (b) per atoms in the unit cell; (c) partial orbits of Sr1, As1, and Sn atoms.

TABLE I: Physical properties of $\text{Sr}_5\text{Sn}_2\text{As}_6$ and $\text{Ca}_5\text{M}_2\text{Sb}_6$ ($M = \text{Al}, \text{Ga}, \text{In}$) compounds: ρ , theoretical density; K , bulk modulus; G , shear modulus; Y , Young's modulus.

M	ρ (g/cm ³)	G (GPa)	K (GPa)	Y (GPa)	ν_s (m/s)	ν_l (m/s)	κ_{min} (W/mK)
$\text{Sr}_5\text{Sn}_2\text{As}_6$	4.99	23	39	58	2147	3749	0.47
$\text{Ca}_5\text{Al}_2\text{Sb}_6$	4.31	25	40	62	2400	4100	0.53
$\text{Ca}_5\text{Ga}_2\text{Sb}_6$	4.52	24	40	60	2280	3970	0.50
$\text{Ca}_5\text{In}_2\text{Sb}_6$	4.90	22	38	55	3710	3710	0.46

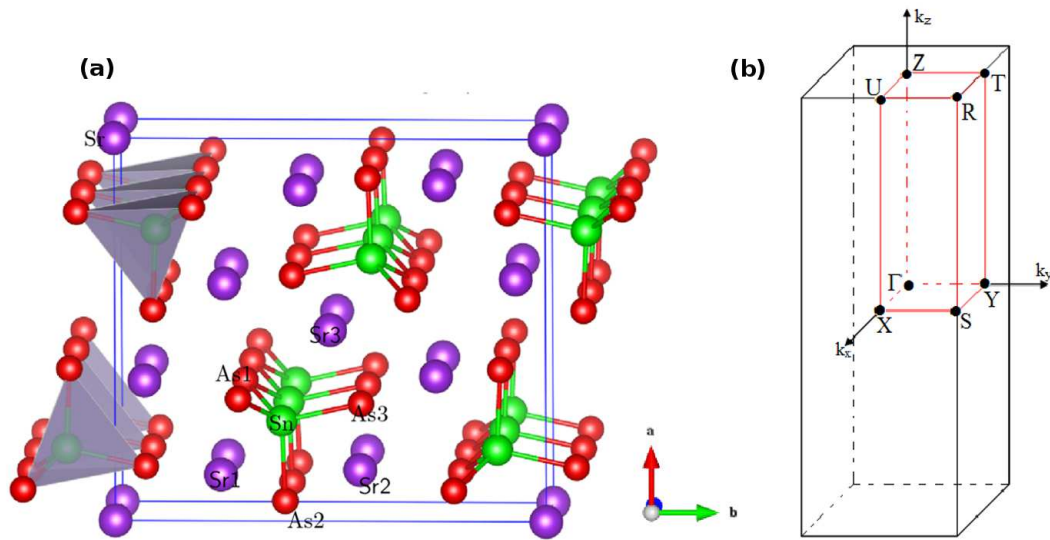


FIG. 1: (a) The optimized crystal structure of $\text{Sr}_5\text{Sn}_2\text{As}_6$. Magenta, red, and green spheres represent Sr, As, and Sn atoms, respectively; (b) The first Brillouin zone (from the primitive unit cell) of $\text{Sr}_5\text{Sn}_2\text{As}_6$.

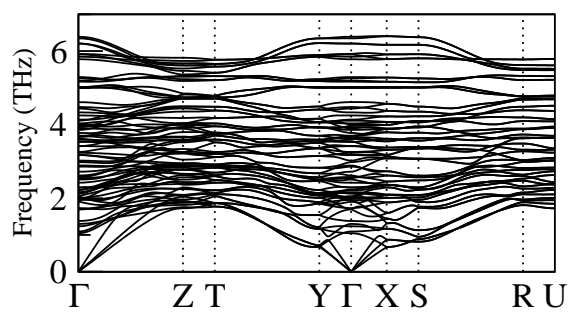


FIG. 2: Phonon dispersion curves of $\text{Sr}_5\text{Sn}_2\text{As}_6$.

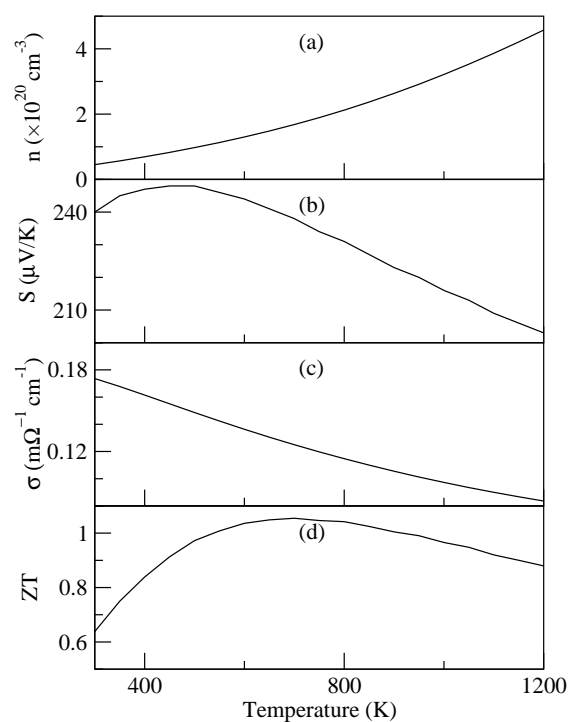


FIG. 3: Calculated thermoelectric properties of $\text{Sr}_5\text{Sn}_2\text{As}_6$ as a function of temperature.

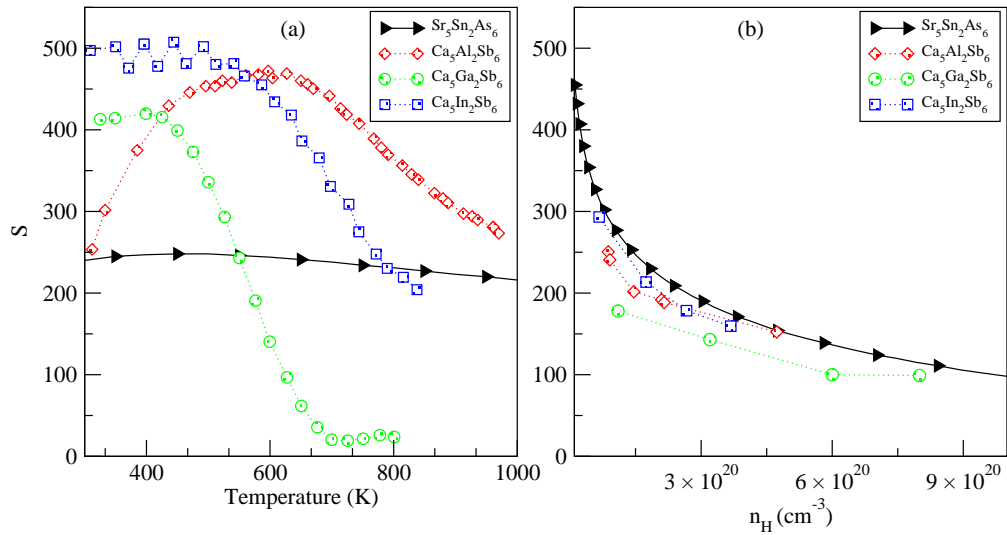


FIG. 4: Seebeck coefficient of $\text{Ca}_5\text{M}_2\text{Sb}_6$ ($M = \text{Al}, \text{Ga}, \text{In}$) in experimental part and $\text{Sr}_5\text{Sn}_2\text{As}_6$ in theory as a function of (a) temperature and (b) carrier concentration at 700 K, respectively. S (unit in $\mu\text{V}/\text{K}$).

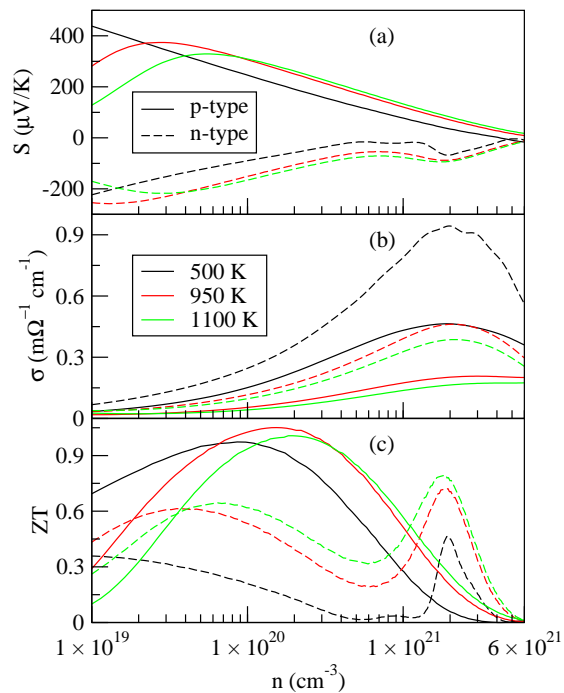


FIG. 5: The calculated thermoelectric properties of p -type and n -type $\text{Sr}_5\text{Sn}_2\text{As}_6$ as a function of carrier concentration from 1×10^{19} to $6 \times 10^{21} \text{ cm}^{-3}$ at 500 K, 950 K, and 1100 K.

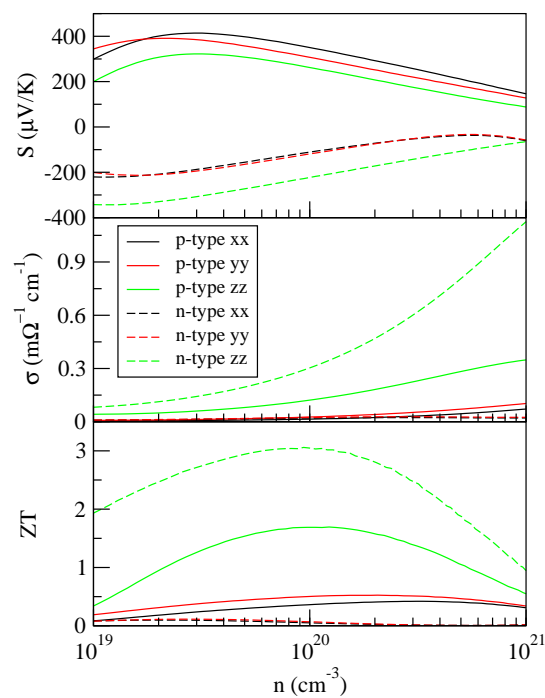


FIG. 6: The thermoelectric anisotropy of $\text{Sr}_5\text{Sn}_2\text{As}_6$ as a function of carrier concentration from 1×10^{19} to $1 \times 10^{21} \text{ cm}^{-3}$ at 950 K.

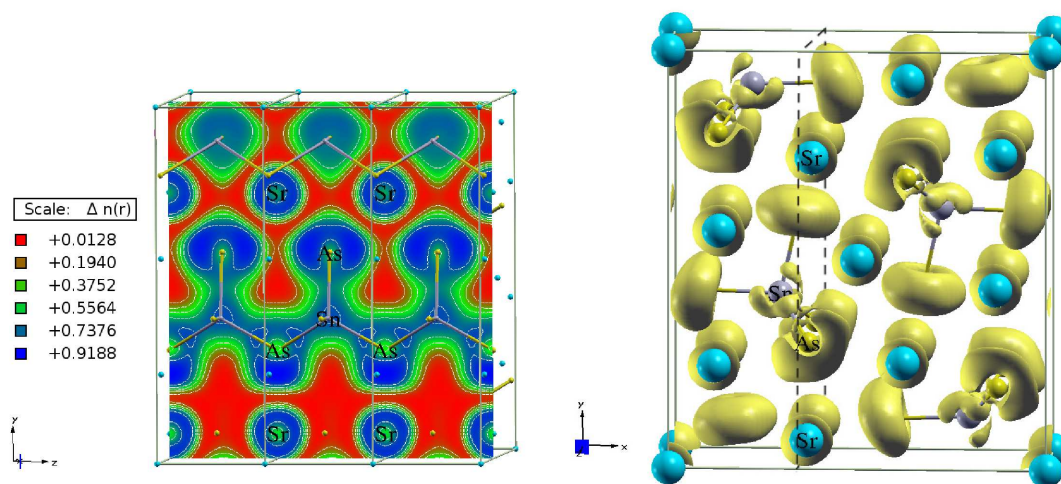


FIG. 7: Calculated electron localization function of $\text{Sr}_5\text{Sn}_2\text{As}_6$ for the (100) plane (left) and the whole unit cell (right) with the isosurface value of 0.78.

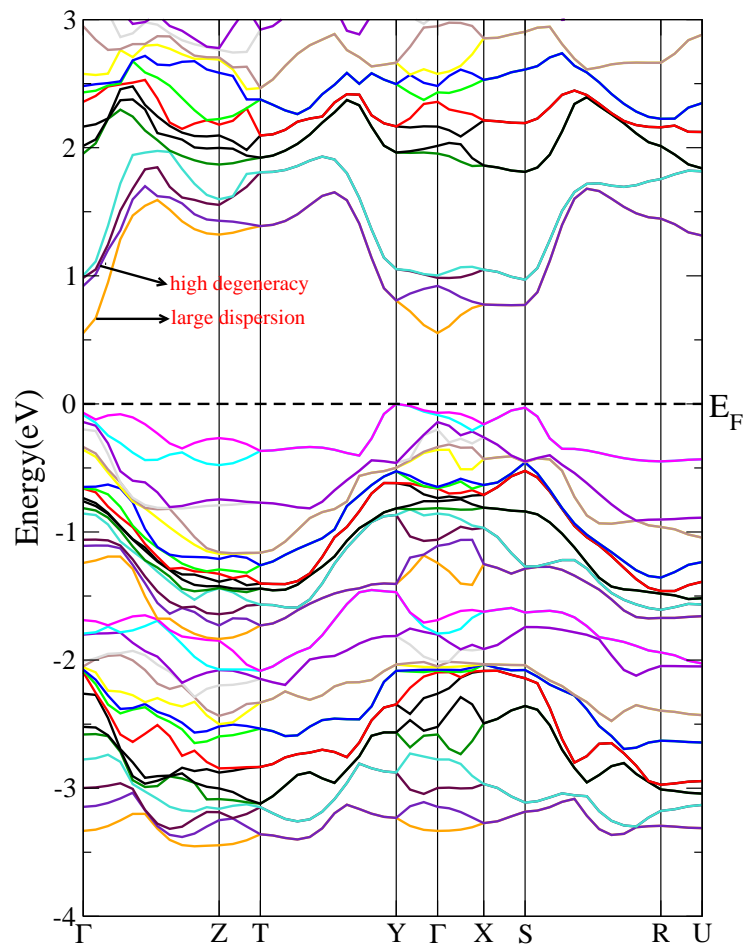


FIG. 8: Calculated band structure of $\text{Sr}_5\text{Sn}_2\text{As}_6$.

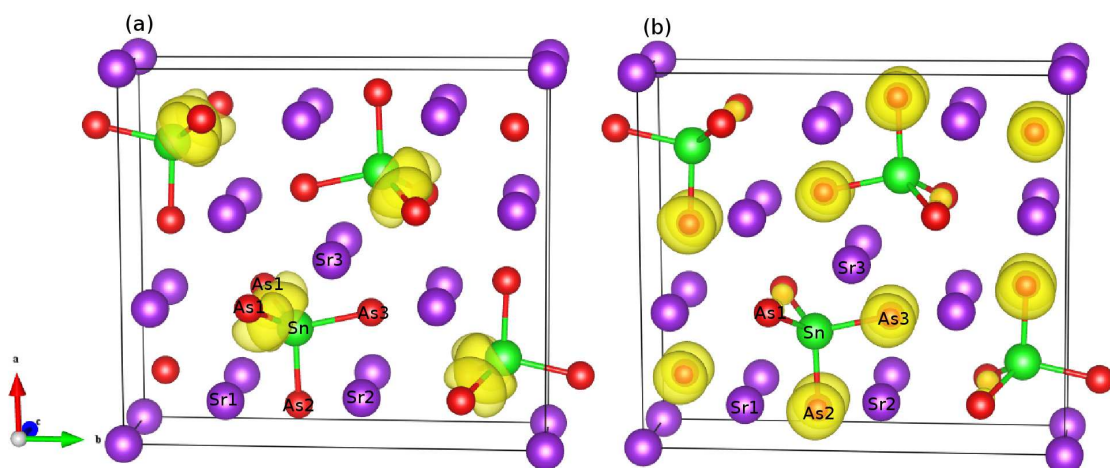


FIG. 9: Band decomposed charge density of (a) conductive bands near the Fermi level at Γ point and (b) valence bands near the Fermi level at Y point for $\text{Sr}_5\text{Sn}_2\text{As}_6$ with the isosurface value of 0.0035.

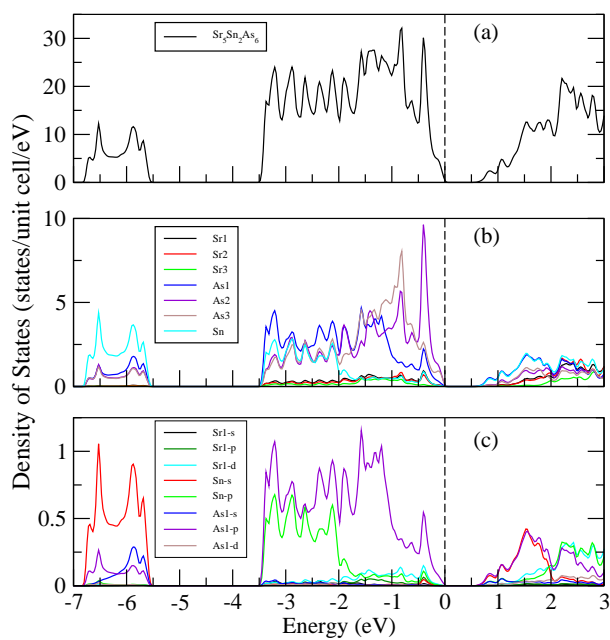


FIG. 10: Calculated projected density-of-states for (a) $\text{Sr}_5\text{Sn}_2\text{As}_6$; (b) per atoms in the unit cell; (c) partial orbits of Sr1, As1, and Sn atoms.

The highest ZT value of n-type $\text{Sr}_5\text{Sn}_2\text{As}_6$ at 950 K appears at a carrier concentration of $9.4 \times 10^{19} \text{ cm}^{-3}$.

